What caused the cold condition over northeast Asia during April 2020?

Go-Un Kim
Korea Institute of Ocean Science and Technology
Hyoeun Oh
Korea Institute of Ocean Science and Technology
Yong Sun Kim
Korea Institute of Ocean Science and Technology
Jun-Hyeok Son
Korea Institute of Ocean Science and Technology
Jin-Yong Jeong (yjeong@kiost.ac.kr)
Korea Institute of Ocean Science and Technology

Article

Keywords:

Posted Date: December 12th, 2022

DOI: https://doi.org/10.21203/rs.3.rs-2335827/v1

Version of Record: A version of this preprint was published at Scientific Reports on February 27th, 2023.
See the published version at https://doi.org/10.1038/s41598-023-29934-w.

Abstract

Northeast Asia has experienced severe damage to agricultural and marine ecosystems due to the cold condition in April 2020, despite the fourth warmest year in northern Asia on record. Previous studies have indicated that the dipole atmospheric circulation over Siberia and the East Sea (Japan Sea) rendered this cold environment, although the cause of atmospheric circulation affecting the cold condition over northeast Asia remains nebulous. Herein we found that the atmospheric structure was a mixed result of the East Atlantic/Western Russia (EAWR) pattern and blocking. The wave train was originated from the vorticity forcing of northwest/central Russia and propagated from western Europe to the East Sea via the background westerly and northerly winds. Besides, the Siberian blocking days increased ten times in April 2020 than climatology along with the easterly anomaly over Mongolia–northeast China. The blocking occurrence was linked to wavy westerly at the high latitudes. The strong blocking and EAWR pattern led to the robust dipole atmospheric structure with the prevailing northerly flow in April 2020, thereby causing the cold over northeast Asia. Our results provide novel insights into the cause of the cold condition in April over northeast Asia and its impact on the land-ocean ecosystems.

Introduction

Extreme weather or climate anomalies can alter the structure of land and ocean ecosystems, as well as species range and timing[1]. Ultimately, ecosystem changes adversely impact food production in agriculture, aquaculture, and fisheries[1]. Humans are exposed to multiple risks under climate change. These hazards have increased through two or more extreme events co-occurring, an extreme event amplifying with climate conditions, or a combination of events leading to extreme event[2–5]. Thus, it is essential to understand the process and cause of unusual weather/climate phenomena to reduce the loss of socio-economic and human activities.

In April 2020, Asia experienced heterogeneous and extreme temperature distribution from region to region. The temperature in the northern region of Asia (Ural and Siberia) was the fourth highest since 1880, while the low temperature was concurrently recorded in northeast Asia (north China and Korea) associated with strong cold advection (www.ncdc.noaa.gov/sotc/global/202004; Fig. 1). This cold condition over northeast Asia occurred within the month of April, ~ 2 days of short-term or ~ 8 days of long-term (Supplementary Fig. S1). The Ministry of Emergency Management of China considered the extreme cold surge during the end of April as one of China's top ten natural disasters in 2020. The severe low-temperature event (minimum temperature of -9°C) damaged 530,000 ha of agricultural produce and negatively affected the lives of 4 million residents living in north and northwest China with a total economic loss of 1.2 billion dollars (www.cma.gov.cn/2011xwzx/2011xmtjj/202101/t20210104_569543.html). Besides, the 22nd April's extreme cold-related sleet was late snowfall in Seoul, South Korea, since record-keeping began in 1907. The Ministry of Agriculture, Food and Rural Affairs of Korea reported that the low-temperature event caused spring frost damage to crops on 48,000 ha, hence the government spent 80 million dollars on recovery efforts (www.mafra.go.kr).

The severe cold environment in April 2020 had negative influence on not only the land of north China and Korea but also the marine ecosystem of the Yellow Sea. Kim et al.[6] identified an unprecedented water temperature evolution over the northeastern basin of the Yellow Sea. The water temperature was 1.2°C higher in March and 1.0°C lower in May 2020 compared with normal years, resulting in the slowest spring temperature evolution in the last four decades. This record-breaking event was principally attributed to the exceptional latent heat releases in April 2020 via robust northwesterly wind, along with warm winter water contributing in part to the air-sea turbulent heat releases at the sea surface. The considerable heat loss from the ocean to the atmosphere generated the cold-water anomaly on the sea surface, while warm anomaly in winter persisted below a thermocline even during spring. The resultant weakened stratification created unfavorable conditions for phytoplankton activity, thus likely affecting the delayed and suppressed spring bloom in 2020. The satellite-derived phytoplankton biomass decreased by ~ 30% over the Yellow Sea in April 2020 than the normal years of 2015–2019[7].

The prevailing northerly wind with cold air mass over northeast Asia tends to occur during the winter season[8–12]. The amplification of the Siberian High mainly explains the cold winter through the upper-tropospheric Rossby wave train and blocking processes[8–12]. By the stationary Rossby wave dynamics, atmospheric waves induced by upper-tropospheric disturbance propagate across the Eurasian. These waves amplify the downstream anticyclonic and cyclonic anomaly circulations through interactions with the pre-existing Siberian high, hence the northerly cold air invaded East Asia[8,10–12]. The blocking pattern process interacts with the complex orography and large-scale circulation variability such as Arctic Oscillation (AO), reinforcing and expanding the Siberian high, and thereby invoking cold air masses to East Asia[9–12]. Interestingly, such cold winter environment seemed to happen during April 2020 in northeast Asia. Previous studies have proposed that the anomalous anticyclonic circulation was located over Siberia, accompanying the cyclonic circulation anomaly over the East Sea (also referred to as the Japan Sea) in April 2020[6,13]. This dipole circulation led to the strong northerly flow resulting in the cold condition in northeast Asia[6,13]. However, the specific cause of the atmospheric dipole structure in April 2020 remains unknown. Therefore, the characteristics and potential causes of the large-scale atmospheric circulation related to the cold condition in April over northeastern Asia need to be examined.

Results

Characteristics of the atmospheric circulation in April 2020

Figure 2 illustrates the 200-, 500-, and 850 hPa geopotential heights, 200 hPa wave activity flux, and blocking frequency anomalies for April 2020 using the European Centre for Medium-Range Weather Forecasts Re-analysis 5 (ERA5). In the east-west (horizontal) direction, the anticyclonic circulation anomalies appeared over western/central Europe (45–60 °N, 5 °W–15 °E) and Siberia (50–70 °N, 80–120 °E) near Lake Baikal. The cyclonic circulations occurred over northwest/central Russia (50–70 °N, 30–60 °E) and the East Sea (25–40 °N, 125–145 °E) with alternating signs (i.e., in a ridge-trough-ridge-trough pattern). Besides, the location of maximum intensity for the anomalous ridge over Siberia/Russian Far

East and the location of minimum intensity for the anomalous trough over the East Sea/northwest Pacific slightly tilted westward with height in the troposphere, in which the vertical structure shows the growth of baroclinic disturbance. This atmospheric circulation structure is analogous to a wave train pattern. The wave activity flux was calculated using Takaya and Nakamura[14] method to estimate the Rossby wave propagation (Fig. 2a green vectors). The wave-flux vector started from western Europe and seemed to proceed towards the marginal northwest Pacific, coincided with the ridge-trough-ridge-trough pattern.

A series of anticyclonic and cyclonic circulation anomalies exhibited over northeast Eurasia in the north-south (meridional) direction. The anomalous ridge over Siberia/Russian far East had a grossly equivalent barotropic vertical structure, but the anomalous trough over the East Sea/northwest Pacific had an apparent westward tilt of about 10° in height. These barotropic ridge and baroclinic trough systems are comparable to a blocking pattern. To identify the blocking occurrence, the blocking days were estimated using the hybrid atmospheric blocking method[15,16], which combines each advantage of the Dole–Gordon index[17] and the Tibaldi–Molteni index[18]. The blocking days over Siberia during April 2020 increased by an area average of 10.6 days than climatology of 1982–2019 (11.6 days up to a maximum of 23 days in 2020 and 1 day in climatology; Supplementary Fig. S2 and Fig. 2b purple contours). These results suggest that the atmospheric structure associated with the cold condition in April 2020 might be attributed to a mixed type of wave train and blocking.

To determine how different the atmospheric circulation related to cold condition in April 2020 compared with normal years, we plotted a scatter diagram of the dipole pattern (ordinate) under the wave train (abscissa) and blocking (maker) indices (Fig. 3). Here, the normal years mean only 17 years occurred the Siberian blocking out of 39 years (in April from 1982 to 2019). The dipole atmospheric circulation index is considered as the cold condition with the northerly flow in northeast Asia. The wave train and blocking indices are potential causes of cold condition (see indices details in the Methods section). During the 17 years, the dipole circulation index showed a positive linear relationship with the wave train index (correlation coefficient = 0.6, $p = 0.01$). The blocking indices with large magnitudes are linked to large wave train and dipole indices as observed in 1997, 2007, 2011, and 2020. In particular, the wave train index in April 2020 was the same as that in 2007 at 3.9, which are the strongest years; however, the dipole index value differed from 4.7 in 2020 and 3 in 2007. This larger dipole index in 2020 seems to reflect the extreme blocking index of 11.6 in 2020 that is the strongest for 39 years, compared with the 6 in 2007. The result reveals that this exceptional Siberian blocking could play a crucial role in modulating the dipole atmospheric circulation over Siberia and the East Sea in concert with the wave train pattern.

Possible Causes For The Cold Condition In April 2020

A question arises as to which forcing can form the atmospheric circulation in April 2020 over Eurasia. To this end, we performed a numerical experiment using the linear baroclinic model (LBM) that is capable of diagnosing the steady-state atmospheric dynamical response to prescribed forcing[19–21]. The experiment

was forced with the robust positive vorticity profile for the northwest/central Russia region from the ERA5 (black box in Fig. 4a and Supplementary Fig. S3) based on the result of wave activity flux. The simulated upper-, mid-, and low-level geopotential height anomalies for near steady-state (averaged over 16–20 days) are plotted in Fig. 4. All tropospheric geopotential height anomalies for the vorticity forcing exhibited horizontally and meridionally alternating positive and negative signs over Eurasia. The spatial correlation between simulated and observed 200 hPa geopotential height was approximately 0.71 over 25–80 °N and 0–150 °E, which was significant at the 99% confidence level. The result indicates that the numerical experiment reasonably reproduces the observed April 2020 of atmospheric circulation. On the other hand, the location of positive height anomalies in western Europe was not well simulated in the model compared to the reanalysis (Figs. 2 and 4), presumably relating to the single effect of north Atlantic or tropics forcing or the complex impact of them[20,22,23].

It is noteworthy that the atmospheric circulation anomalies in the horizontal direction have an arc-shaped wave pattern (Fig. 4). The ray tracing method was applied to identify a path of the Rossby wave propagation. The calculated rays for zonal wavenumber 2 matched well with the centers of upper-tropospheric geopotential height anomalies (navy lines and yellow squares in Fig. 4a), implying the vorticity forcing at northwest/central Russia could generate the teleconnection pattern toward the marginal northwest Pacific. This wave energy propagation was possible since the modified Rossby wave theory considers the effect of basic zonal and meridional wind[19,24–26](Fig. 5a and Supplementary Fig. S4). In climatology, the meridional vorticity gradient showed a positive value across 40–60 °N and 30–120 °E (Fig. 5a), which was proportional to the polar front westerly[27,28] and the northerly wind over Ural-Siberia (Supplementary Fig. S4). Along the westerly and northerly background flows that are included in the dispersion relationship for the barotropic Rossby wave, the stationary wave penetrated southeastward into the East Sea.

This wave train pattern is analogous to the East Atlantic/Western Russia (EAWR) teleconnection. The EAWR pattern is one of the most dominant atmospheric teleconnections that affect the weather and climate in Eurasian throughout the year[29–34]. The positive phase of the EAWR pattern has positive height anomalies over Europe and northern China and negative over the central North Atlantic and north of the Caspian Sea, and vice versa. External and internal forcing could generate and maintain atmospheric wave trains in mid-latitude[19,29,32,33,35,36]. As external forcing factor, anomalous boundary condition such as North Atlantic Sea surface temperature and North American/Eurasian snow cover could induce the upper-level divergence wind, acting as the Rossby wave source for the EAWR pattern[32,33,35]. Also, as internal dynamics, the interaction between background westerly and synoptic-scale transient eddies could drive the atmospheric Rossby wave energy propagation from the North Atlantic[29,33]. The spatial map of 200 hPa geopotential height anomalies was regressed against the EAWR index for 1982–2020 (Supplementary Fig. S5). This height regression field with the EAWR index showed a consistent pattern to the observation of the geopotential height anomaly in April 2020 (Fig. 2a). The EAWR index exhibited a strong positive correlation coefficient of 0.89 with the wave train index (defined the index in this study) for

39 years, suggesting that the EAWR pattern accounts for approximately 79% of the year-to-year variance of wave train patterns.

In the meridional direction, the barotropic high-pressure anomaly over Siberia appeared with the baroclinic low-pressure anomaly over the East Sea, similar to the observed blocking pattern (Fig. 4). The atmospheric blocking system was closely connected with the wind speed variation in upper-level troposphere. The 200 hPa zonal winds showed the strong negative anomaly (i. e., easterly anomaly wind) over the Mongolia–northeast China in April 2020 compared with climatology, but strong positive anomaly over the northern Russia and southern China (Fig. 5b). The wind structure of positive-negative-positive anomalies near 120 °E corresponded with anomalous anticyclone and cyclone over Siberia and the East Sea, respectively. Furthermore, the zonal wind anomaly exhibited a wave-like pattern over 40–80 °N, resembling the distribution of blocking frequency anomaly (Fig. 5b and Supplementary Fig. S2c): anomalous easterly/westerly wind region coincided with reduced/increased blocking frequency area. This result indicates that the Siberian blocking is relevant to the Rossby wave train pattern over Eurasia[9,14,37,38]. As shown in Fig. 4a, the Rossby wave train transferred the wave energy from upstream of Europe to downstream of Asia; this convergence of wave activity flux can reinforce and rebuild the anticyclonic circulation over Siberia; thus, likely creating a more intense and persistent blocking.

Summary And Discussion

This study elucidates that the causes of the dipole atmospheric circulation over Siberia and the East Sea associated with the cold condition in April 2020 in northeast Asia. The anomalous ridge and trough structure were a mixed pattern of stationary Rossby wave train and blocking. The wave train with alternating anticyclonic and cyclonic circulations across Eurasia was induced by the vorticity forcing of northwest/central Russia and propagated from western Europe to the East Sea. The climatological polar front jet and northerly wind allowed the wave energy to propagate toward the southeast. This wave pattern almost corresponds to the EAWR teleconnection pattern, one of the influential atmospheric circulations in Eurasian weather. In addition, the blocking frequency increased by approximately ten times over Siberia in April 2020 than that of climatology. This Siberia region of increased blocking days nearly paralleled the weaker westerly wind in April 2020 over Mongolia–northeast China. The change in blocking frequency distribution was related to the wavy zonal flow change across the high latitude, similar to the Rossby wave response[9,14,37,38]. The propagating/breaking Rossby wave might reestablish and re-strengthen the blocking high.

The reason that the Siberian blocking frequency in April 2020 was the strongest over the past 39 years remains still unclear. Many previous studies demonstrated that the Siberian blocking tends to occur in stronger and longer cold condition over East Asia during the negative AO period in winter[10,11,39–42]. However, no relationship between blocking and AO was identified in April 2020; the AO index was positive (0.93), while the blocking index had the highest value of 11.6 days. For the winter and early spring of 2020 (January–March) in the last four decades, the positive AO accompanied by the exceptional

stratospheric polar vortex was extraordinarily robust at 2.83[43]. This record low-frequency variability enabled maintaining the pattern of the cold Arctic and warm Eurasia until March 2020 through the strengthened westerly flow. Then, the AO index became weaker in April and more neutral in May (-0.03) than during January–March, coinciding with the change in westerly circulation surrounding the Arctic (Fig. 5b). We suggest a link between the blocking over Siberia and the AO phase transition from an extreme positive value in January–March to a weak negative value in May (from 2.83 to -0.03). Thus, further study is warranted to clarify the relationship between the blocking and AO phase transition in springtime.

Our study highlights that extreme Siberian blocking and strong EAWR pattern influenced the dipole atmospheric circulation causing the cold condition in northeast Asia in April 2020. This cold condition seriously harmed agricultural and marine ecosystems over northeastern Asia during the peak growth period, such as fruit trees blossom, farm sprout, and phytoplankton spring bloom[6] (www.cma.gov.cn and www.mafra.go.kr). Therefore, the current results will be helpful for better understanding the extreme weather or climate over northeastern Asia in April and its damage to the land-ocean ecosystems.

Methods

Reanalysis data

We used the monthly and daily mean data for 39 years—from 1982 to 2020 from the ERA5[44]. The reanalysis data have a 0.25° × 0.25° longitude-latitude grid at 37 vertical pressure levels for the atmospheric variables. The 2020 anomalies for each variable were calculated by removing the climatology mean from 1982 to 2019. The indices in this study were: the dipole atmospheric circulation index as the normalized geopotential height of 500 hPa anomalies averaged over Siberia (50–70 °N, 80–120 °E) minus the East Sea (25–40 °N, 125–145 °E), which is an important factor relevant to the April cold condition over northeast Asia; the wave train index as the normalized geopotential height of 500 hPa anomalies averaged over western/central Europe (45–60 °N, 5 °W–15 °E) minus northwest/central Russia (50–70 °N, 30–60 °E); the blocking index as the sum of the total number of blocking frequencies per month over Siberia (indicated by the boxes in Fig. 2c). We also used the EAWR and AO indices from the website of National Oceanic and Atmospheric Administration Climate Prediction Center.

Model Configuration And Experiment Design

This study employed the linear baroclinic model LBM[45] to investigate the circulation response to imposed vorticity forcing, which causes the large-scale atmospheric circulation over Eurasia[19–21]. The model had a horizontal resolution of T42 and 20 vertical sigma levels based on the linearized primitive equations. The numerical experiment was performed using the profile over the northwest/central Russia region with strong vorticity forcing (Supplementary Fig. S3). The background state in the experiments was set to the

April climatological field taken from the ERA5, which includes geopotential height, relative humidity, specific humidity, temperature, three-dimensional winds, and sea level pressure.

Ray Tracing

We applied the ray tracing method to analyze the pathway of Rossby wave energy propagation generated by the vorticity forcing[24–26, 46,47]. The dispersion relationship for barotropic nondivergence wave in a non-uniform basic horizontal flow with a meridional wind component[24,25] is presented as

$$\omega = \bar{u}_M k + \bar{v}_M l + \frac{\bar{q}_x l - \bar{q}_y k}{K^2}$$

where, $\bar{q}_x$ and $\bar{q}_y$ are the zonal and meridional gradients of absolute vorticity, respectively, and expressed as

$$\bar{q}_x = \frac{1}{a^2 cos\varphi}\left(\frac{\partial^2 \bar{v}}{\partial \lambda^2} - \frac{\partial^2 \bar{u}}{\partial \lambda \partial \varphi} cos\varphi + \frac{\partial \bar{u}}{\partial \lambda} sin\varphi\right) \text{ and } \bar{q}_y = \bar{\beta}_M + \frac{\partial^2 \bar{v}}{\partial \lambda \partial \varphi} + tan\varphi \frac{\partial \bar{v}}{\partial \lambda}$$

where $\bar{\beta}_M$ is the poleward absolute vorticity gradient of $\frac{\partial f}{\partial y} - \frac{\partial^2 \bar{u}_M}{\partial y^2}$; $\bar{u}_M$ and $\bar{v}_M$ are the background zonal and meridional flow on a Mercator projection, respectively; k and l are the zonal and meridional wavenumber; ω is the frequency, where $\omega = 0$ denotes the case of the stationary Rossby wave. A more detailed description of this dispersion relationship has been previously reported by Li et al.[24] and Zhao et al.[25].

Blocking Frequency

The hybrid blocking frequency detection is a suitable method for the detection of atmospheric blocking using long-term datasets[15,16]. This blocking method combines the advantages of the most commonly used blocking indices, i.e., the Dole–Gordon index[17] and the Tibaldi–Molteni index[18]. The hybrid approach can detect blocking systems accurately by considering a meridional gradient reversal to reduce the erroneous classification of blocking (such as excluding a misdetection of quasi-stationary high-pressure and including an omega-shaped blocking). To detect the event of hybrid blocking, we followed the four-step procedure described by Dunn-Sigouin et al[15]. Step 1: The 500 hPa geopotential height anomaly was defined as $Z' = Z - \bar{Z} - \widehat{Z}$[48], where Z is the normalized geopotential height by the sine of latitude, $\bar{Z}$ is the running annual mean of Z on a given day, and $\widehat{Z}$ is the seasonal mean cycle derived from the running monthly mean of $Z - \bar{Z}$. Step 2: The closed contour of the blocking anomaly (positive Z') was identified using spatial criteria based on the minimum amplitude and spatial scale, and temporal criteria based on minimum overlap in the blocking area within two days. The minimum amplitude threshold was set to 1.5 of a standard deviation of Z' over 30–90 °N for an average of three months

centered on a given month. The spatial scale threshold was 2.5×10^6 km^2, with a minimum overlap threshold of 50%. Step 3: The closed contour of the blocking anomaly should also satisfy the absolute meridional Z gradient's reversal. Step 4: If the conditions in steps 2 and 3 were ensured for five consecutive days, the blocking anomaly would be referred to as an atmospheric blocking high.

Declarations

Acknowledgements

This research was supported by Korea Institute of Marine Science & Technology Promotion (KIMST) funded by the Ministry of Oceans and Fisheries (20210607, Establishment of the Ocean Research Station in the Jurisdiction Zone and Convergence Research) and the National Research Foundation of Korea (NRF) grant funded by the Korea government (MSIT) (No. 2021R1C1C2005002).

Author contributions

G.-U.K., Y.S.K., and J.-Y.J. conceptualized the research. G.-U.K, H.O., Y.S.K., and J.-H.S. interpreted and discussed the results. G.-U.K. performed model runs, and wrote the first draft of the manuscript. All authors contributed to improving the manuscript.

Data availability

All data are publicly available from the following sites: ERA5 monthly and daily data at https://cds.climate.copernicus.eu.; EAWR and AO indices at https://www.cpc.ncep.noaa.gov/; LBM source code at https://ccsr.aori.u-tokyo.ac.jp/~lbm/sub/lbm.html. Simulated LBM data is available from the corresponding author on reasonable request.

References

1. IPCC. Summary for Policymakers [H.-O. Pörtner, D.C. Roberts, E.S. Poloczanska, K. Mintenbeck, M. Tignor, A. Alegría, M. Craig, S. Langsdorf, S. Löschke, V. Möller, A. Okem (eds.)] In: *Climate Change 2022: Impacts, Adaptation, and Vulnerability*. Contribution of Working Group II to the Sixth Assessment Report of the Intergovernmental Panel on Climate Change [H.-O. Pörtner, D.C. Roberts, M. Tignor, E.S. Poloczanska, K. Mintenbeck, A. Alegría, M. Craig, S. Langsdorf, S. Löschke, V. Möller, A. Okem, B. Rama (eds.)]. Cambridge University Press, Cambridge, UK and New York, NY, USA, pp. 3-33, doi:10.1017/9781009325844.001 (2022).
2. Im, E. S., Pal, J. S. & Eltahir, E. A. Deadly heat waves projected in the densely populated agricultural regions of South Asia. *Sci. Adv.* **3**, e1603322 (2017).
3. Wu, X., Hao, Z., Hao, F. & Zhang, X. Variations of compound precipitation and temperature extremes in China during 1961-2014. *Sci. Total Environ.* **663**, 731-737, doi:10.1016/j.scitotenv.2019.01.366

(2019).

4. Zscheischler, J. *et al.* A typology of compound weather and climate events. *Nat. Rev. Earth Environ.* **1**, 333-347, doi:10.1038/s43017-020-0060-z (2020).
5. Ha, K.-J. *et al.* Dynamics and characteristics of dry and moist heatwaves over East Asia. *npj Clim. Atmos. Sci.* **5**, doi:10.1038/s41612-022-00272-4 (2022).
6. Kim, G.-U. *et al.* Record-Breaking Slow Temperature Evolution of Spring Water During 2020 and Its Impacts on Spring Bloom in the Yellow Sea. *Front. Mar. Sci.* **9**, doi:10.3389/fmars.2022.824361 (2022).
7. Yoon, J. E., Son, S. & Kim, I. N. Capture of decline in spring phytoplankton biomass derived from COVID-19 lockdown effect in the Yellow Sea offshore waters. *Mar. Pollut. Bull.* **174**, 113175, doi:10.1016/j.marpolbul.2021.113175 (2022).
8. Takaya, K. & Nakamura, H. Mechanisms of Intraseasonal Amplification of the Cold Siberian High. *J. Atmos. Sci.* **62**, 4423-4440, doi:10.1175/jas3629.1 (2005).
9. Takaya, K. & Nakamura, H. Geographical Dependence of Upper-Level Blocking Formation Associated with Intraseasonal Amplification of the Siberian High. *J. Atmos. Sci.* **62**, 4441-4449, doi:10.1175/jas3628.1 (2005).
10. Park, T.-W., Ho, C.-H. & Deng, Y. A synoptic and dynamical characterization of wave-train and blocking cold surge over East Asia. *Clim. Dyn.* **43**, 753-770, doi:10.1007/s00382-013-1817-6 (2014).
11. Park, T.-W., Ho, C.-H., Jeong, J.-H., Heo, J.-W. & Deng, Y. A new dynamical index for classification of cold surge types over East Asia. *Clim. Dyn.* **45**, 2469-2484, doi:10.1007/s00382-015-2483-7 (2015).
12. Lu, M.-M. & Chang, C.-P. Unusual Late-Season Cold Surges during the 2005 Asian Winter Monsoon: Roles of Atlantic Blocking and the Central Asian Anticyclone. *J. Clim.* **22**, 5205-5217, doi:10.1175/2009jcli2935.1 (2009).
13. Yu, H. *et al.* Attribution of April 2020 Exceptional Cold Spell over Northeast China. *Bull. Am. Meteorol. Soc.* **103**, S61-S67, doi:10.1175/bams-d-21-0175.1 (2022).
14. Takaya, K. & Nakamura, H. A Formulation of a Phase-Independent Wave-Activity Flux for Stationary and Migratory Quasigeostrophic Eddies on a Zonally Varying Basic Flow. *J. Atmos. Sci.* **58**, 608-627, doi:10.1175/1520-0469(2001)058<0608:afoapi>2.0.co;2 (2001).
15. Dunn-Sigouin, E., Son, S.-W. & Lin, H. Evaluation of Northern Hemisphere Blocking Climatology in the Global Environment Multiscale Model. *Mon. Weather Rev.* **141**, 707-727, doi:10.1175/mwr-d-12-00134.1 (2013).
16. Kim, S.-H. & Ha, K.-J. Two leading modes of Northern Hemisphere blocking variability in the boreal wintertime and their relationship with teleconnection patterns. *Clim. Dyn.* **44**, 2479-2491, doi:10.1007/s00382-014-2304-4 (2015).
17. Dole, R. M. & Gordon, N. D. Persistent Anomalies of the Extratropical Northern Hemisphere Wintertime Circulation: Geographical Distribution and Regional Persistence Characteristics. *Mon. Weather Rev.* **111**, 1567-1586, doi:10.1175/1520-0493(1983)111<1567:paoten>2.0.co;2 (1983).

18. Tibaldi, S. & Molteni, F. On the operational predictability of blocking. *Tellus A: Dyn. Meteorol. Oceanogr.* **42**, 343-365, doi:10.3402/tellusa.v42i3.11882 (1990).
19. Kim, G.-U., Seo, K.-H. & Chen, D. Climate change over the Mediterranean and current destruction of marine ecosystem. *Sci. Rep.* **9**, 18813, doi:10.1038/s41598-019-55303-7 (2019).
20. Son, J.-H., Seo, K.-H., Son, S.-W. & Cha, D.-H. How Does Indian Monsoon Regulate the Northern Hemisphere Stationary Wave Pattern? *Front. Earth Sci.* **8**, doi:10.3389/feart.2020.599745 (2021).
21. Kim, J.-H., Kim, S.-J., Kim, J.-H., Hayashi, M. & Kim, M.-K. East Asian heatwaves driven by Arctic-Siberian warming. *Sci. Rep.* **12**, doi:10.1038/s41598-022-22628-9 (2022).
22. Ok, J. *et al.* How does the SST variability over the western North Atlantic Ocean control Arctic warming over the Barents–Kara Seas? *Environ. Res. Lett.* **12**, 034021 (2017).
23. Li, R. K. K., Woollings, T., O'Reilly, C. & Scaife, A. A. Tropical atmospheric drivers of wintertime European precipitation events. *Q. J. R. Meteorol. Soc.* **146**, 780-794, doi:10.1002/qj.3708 (2020).
24. Li, Y., Li, J., Jin, F. F. & Zhao, S. Interhemispheric Propagation of Stationary Rossby Waves in a Horizontally Nonuniform Background Flow. *J. Atmos. Sci.* **72**, 3233-3256, doi:10.1175/jas-d-14-0239.1 (2015).
25. Zhao, S., Li, J. & Li, Y. Dynamics of an Interhemispheric Teleconnection across the Critical Latitude through a Southerly Duct during Boreal Winter. *J. Clim.* **28**, 7437-7456, doi:10.1175/jcli-d-14-00425.1 (2015).
26. Lee, H.-J. & Jin, E.-K. Seasonality and Dynamics of Atmospheric Teleconnection from the Tropical Indian Ocean and the Western Pacific to West Antarctica. *Atmosphere* **12**, 849, doi:10.3390/atmos12070849 (2021).
27. Huang, D.-Q., Zhu, J., Zhang, Y.-C., Wang, J. & Kuang, X.-Y. The Impact of the East Asian Subtropical Jet and Polar Front Jet on the Frequency of Spring Persistent Rainfall over Southern China in 1997–2011. *J. Clim.* **28**, 6054-6066, doi:10.1175/jcli-d-14-00641.1 (2015).
28. Chowdary, J. S. *et al.* The Eurasian Jet Streams as Conduits for East Asian Monsoon Variability. *Curr. Clim. Change Rep.* **5**, 233-244, doi:10.1007/s40641-019-00134-x (2019).
29. Lim, Y.-K. The East Atlantic/West Russia (EA/WR) teleconnection in the North Atlantic: climate impact and relation to Rossby wave propagation. *Clim. Dyn.* **44**, 3211-3222, doi:10.1007/s00382-014-2381-4 (2015).
30. Gao, T., Yu, J.-Y. & Paek, H. Impacts of four northern-hemisphere teleconnection patterns on atmospheric circulations over Eurasia and the Pacific. *Theor. Appl. Climatol.* **129**, 815-831, doi:10.1007/s00704-016-1801-2 (2017).
31. Barnston, A. G. & Livezey, R. E. Classification, Seasonality and Persistence of Low-Frequency Atmospheric Circulation Patterns. *Mon. Weather Rev.* **115**, 1083-1126, doi:10.1175/1520-0493(1987)115<1083:csapol>2.0.co;2 (1987).
32. Liu, Y., Wang, L., Zhou, W. & Chen, W. Three Eurasian teleconnection patterns: spatial structures, temporal variability, and associated winter climate anomalies. *Clim. Dyn.* **42**, 2817-2839, doi:10.1007/s00382-014-2163-z (2014).

33. Chen, S., Wu, R., Chen, W., Hu, K. & Yu, B. Structure and dynamics of a springtime atmospheric wave train over the North Atlantic and Eurasia. *Clim. Dyn.* **54**, 5111-5126, doi:10.1007/s00382-020-05274-7 (2020).
34. Oh, H., Jhun, J.-G., Ha, K.-J. & Seo, K.-H. Combined effect of the East Atlantic/West Russia and Western Pacific teleconnections on the East Asian winter monsoon. *Asia-Pac. J. Atmos. Sci.* **53**, 273-285, doi:10.1007/s13143-017-0030-7 (2017).
35. Chen, S., Wu, R. & Liu, Y. Dominant Modes of Interannual Variability in Eurasian Surface Air Temperature during Boreal Spring. *J. Clim.* **29**, 1109-1125, doi:10.1175/jcli-d-15-0524.1 (2016).
36. Son, J.-H., Seo, K.-H. & Wang, B. How Does the Tibetan Plateau Dynamically Affect Downstream Monsoon Precipitation? *Geophys. Res. Lett.* **47**, doi:10.1029/2020gl090543 (2020).
37. Sung, M.-K., Lim, G.-H., Kug, J.-S. & An, S.-I. A linkage between the North Atlantic Oscillation and its downstream development due to the existence of a blocking ridge. *J. Geophys. Res.* **116**, doi:10.1029/2010jd015006 (2011).
38. Trenberth, K. E. & Fasullo, J. T. Climate extremes and climate change: The Russian heat wave and other climate extremes of 2010. *J. Geophys. Res. Atmos.* **117**, doi:10.1029/2012jd018020 (2012).
39. Park, T.-W., Ho, C.-H. & Yang, S. Relationship between the Arctic Oscillation and Cold Surges over East Asia. *J. Clim.* **24**, 68-83, doi:10.1175/2010jcli3529.1 (2011).
40. Cheung, H. H. N. *et al.* A strong phase reversal of the Arctic Oscillation in midwinter 2015/2016: Role of the stratospheric polar vortex and tropospheric blocking. *J. Geophys. Res. Atmos.* **121**, 13,443-413,457, doi:10.1002/2016jd025288 (2016).
41. Yeo, J.-H. & Ha, K.-J. Combined Effects of Blocking and AO on a Prolonged Snowstorm in Jeju Island. *Asia-Pac. J. Atmos. Sci.* **55**, 401-414, doi:10.1007/s13143-018-0088-x (2019).
42. Park, T.-W., Ho, C.-H., Yang, S. & Jeong, J.-H. Influences of Arctic Oscillation and Madden-Julian Oscillation on cold surges and heavy snowfalls over Korea: A case study for the winter of 2009–2010. *J. Geophys. Res.* **115**, doi:10.1029/2010jd014794 (2010).
43. Lawrence, Z. D. *et al.* The Remarkably Strong Arctic Stratospheric Polar Vortex of Winter 2020: Links to Record-Breaking Arctic Oscillation and Ozone Loss. *J. Geophys. Res. Atmos.* **125**, doi:10.1029/2020jd033271 (2020).
44. Hersbach, H. *et al.* The ERA5 global reanalysis. *Q. J. R. Meteorol. Soc.* **146**, 1999-2049, doi:10.1002/qj.3803 (2020).
45. Watanabe, M. & Kimoto, M. Atmosphere-ocean thermal coupling in the North Atlantic: A positive feedback. *Q. J. R. Meteorol. Soc.* **126**, 3343-3369, doi:10.1002/qj.49712657017 (2000).
46. Hoskins, B. J. & Ambrizzi, T. Rossby Wave Propagation on a Realistic Longitudinally Varying Flow. *J. Atmos. Sci.* **50**, 1661-1671, doi:10.1175/1520-0469(1993)050<1661:rwpoar>2.0.co;2 (1993).
47. Seo, K.-H. & Lee, H.-J. Mechanisms for a PNA-Like Teleconnection Pattern in Response to the MJO. *J. Atmos. Sci.* **74**, 1767-1781, doi:10.1175/jas-d-16-0343.1 (2017).

48. Sausen, R., König, W. & Sielmann, F. Analysis of blocking events from observations and ECHAM model simulations. *Tellus A: Dyn. Meteorol. Oceanogr.* **47**, 421-438, doi:10.3402/tellusa.v47i4.11526 (1995).

Figures

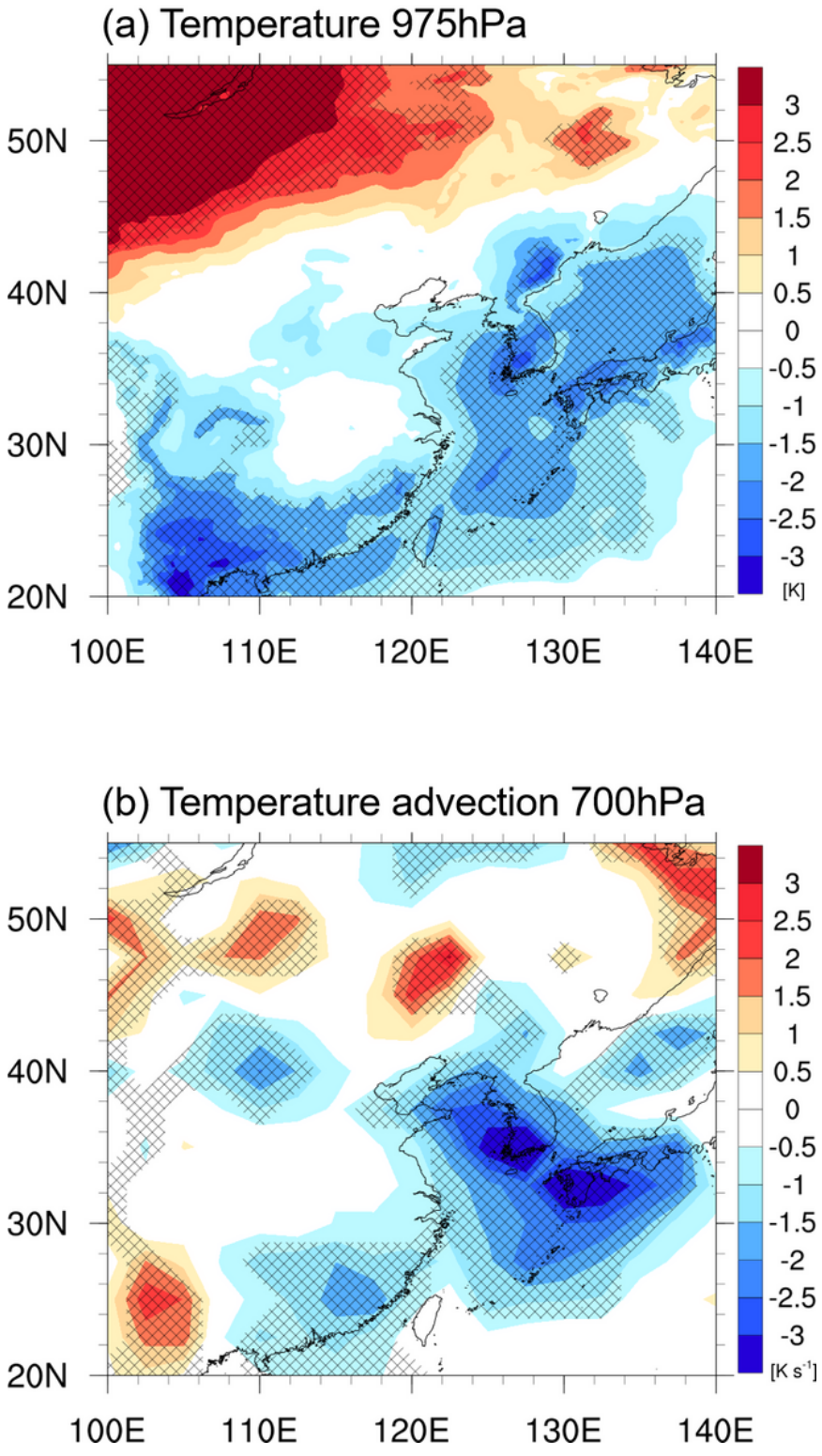

Figure 1

Maps of cold condition in April 2020. Spatial patterns of (a) 975-hPa temperature (shading, K) and (b) 700-hPa temperature advection anomalies (shading, 10^{-5} K s^{-1}) in April 2020 for the ERA5. Hatched areas denote the statistically significant regions at the 90% confidence level.

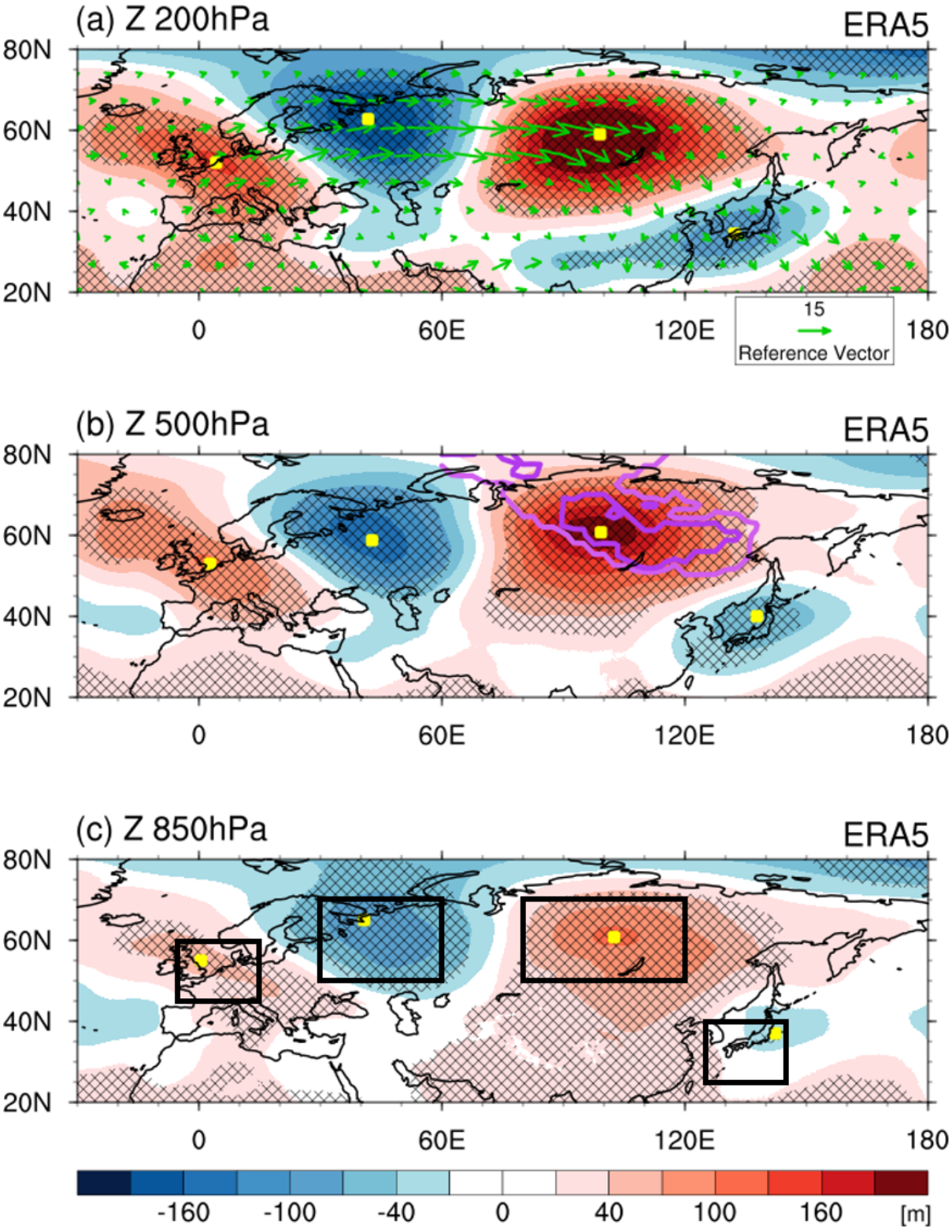

Figure 2

Characteristics of atmospheric circulation anomalies in April 2020. Spatial maps of (a) 200 hPa, (b) 500 hPa, and (c) 850 hPa geopotential height (shading, m), 200 hPa wave activity flux (vector, m^2 s^{-2}), and blocking frequency (contour, days $month^{-1}$) anomalies in April 2020 for the ERA5. Yellow squares indicate the location where the maximum or minimum geopotential height anomalies. Hatched areas denote the statistically significant regions at the 90% confidence level. In (a), reference wave activity flux vector is 15 m^2 s^{-2}. Light and dark purple contours in (b) are the area of more than 14- and 16-days per month of occurring blocking frequency in April 2020 compared with climatology. In (c), black boxes are the regional domains information for the three indices from left to right: western/central Europe (45–60 °N, 5 °W–15 °E), northwest/central Russia (50–70 °N, 30–60 °E), Siberia (50–70 °N, 80–120 °E), and the East Sea (25–40 °N, 125–145 °E).

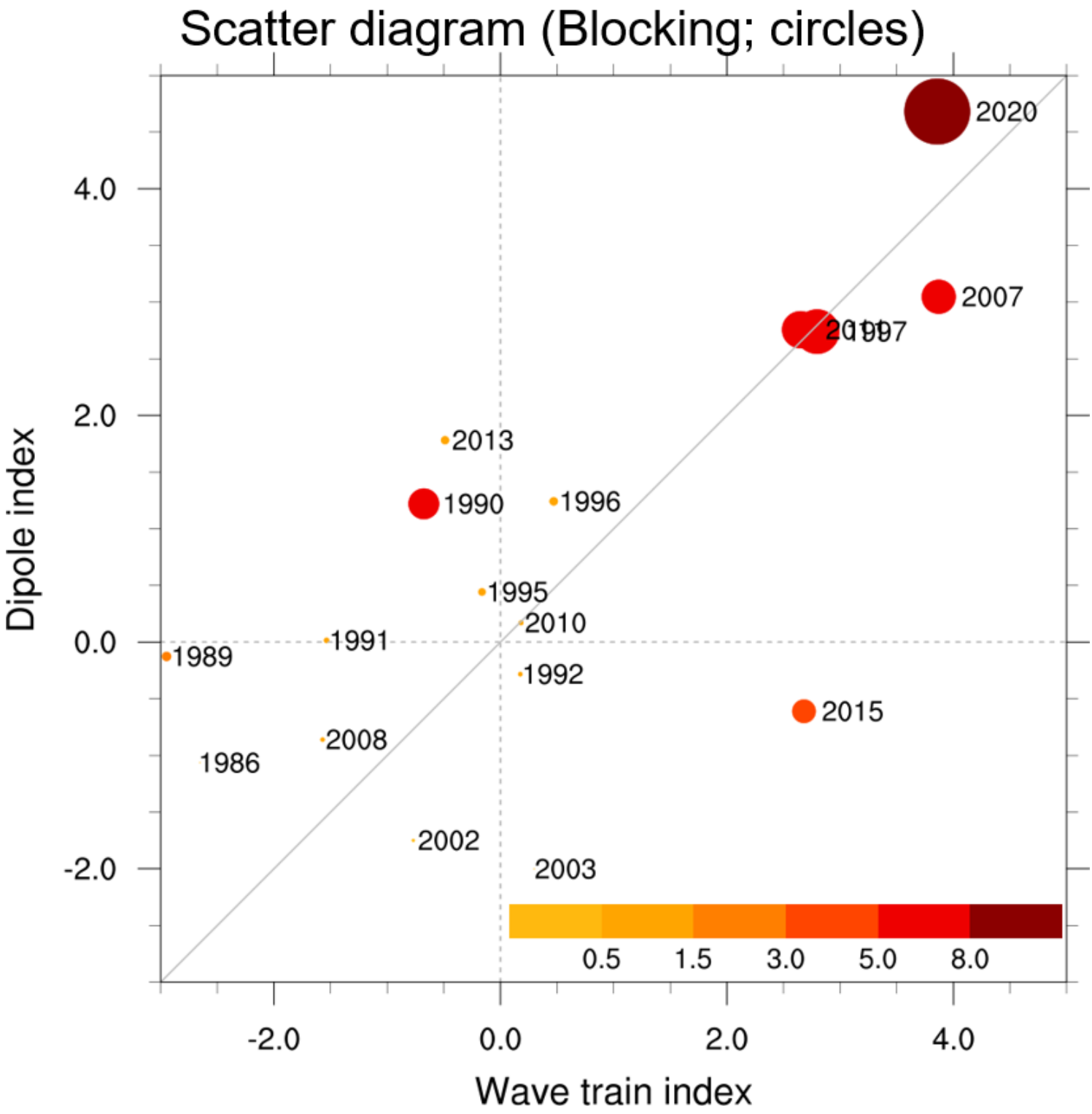

Figure 3

Comparison between April 2020 and normal years on the atmospheric circulation linked to the cold condition. Scatter diagram of the wave train index (*x*-axis) under dipole index (*y*-axis) and blocking index (circles) during April 1982–2020, except for the year with a zero-blocking index (i. e., non-blocking). Each circle's size and color (from yellow to red) denote the magnitude of the blocking index, indicating the blocking frequency in Siberia. Each year is presented on the right side of circles.

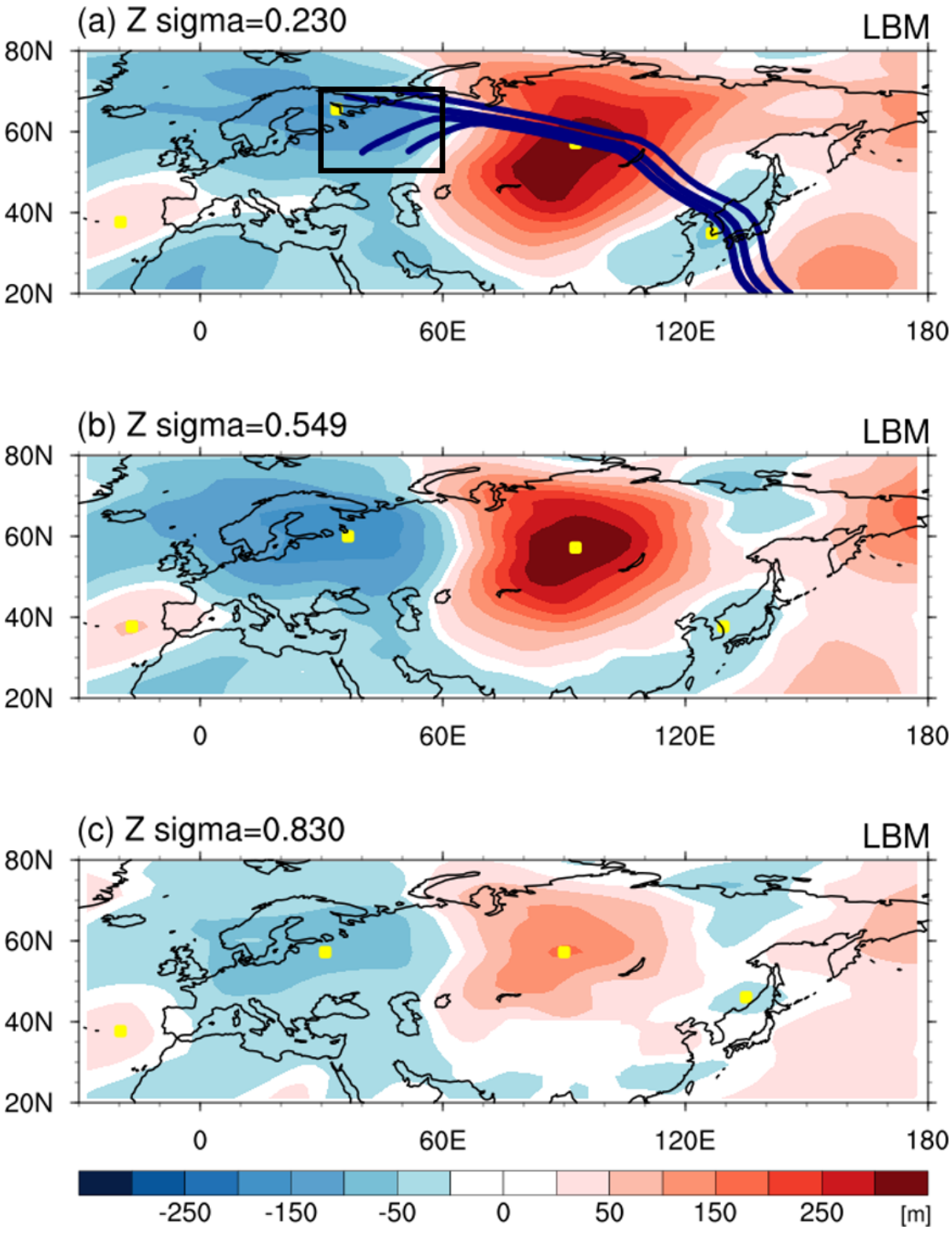

Figure 4

Simulated atmospheric circulation anomalies in response to vorticity forcing. (a) 0.230σ, (b) 0.549σ, and (c) 0.830σ geopotential height anomalies (shading, m) averaged over 16–20 days of output in response to vorticity forcing. In (a), navy lines represent the Rossby wave ray path for waves with the zonal wavenumber 2, while the black box indicates the vorticity forcing region (northwest/central Russia; 50–70 °N, 30–60 °E).

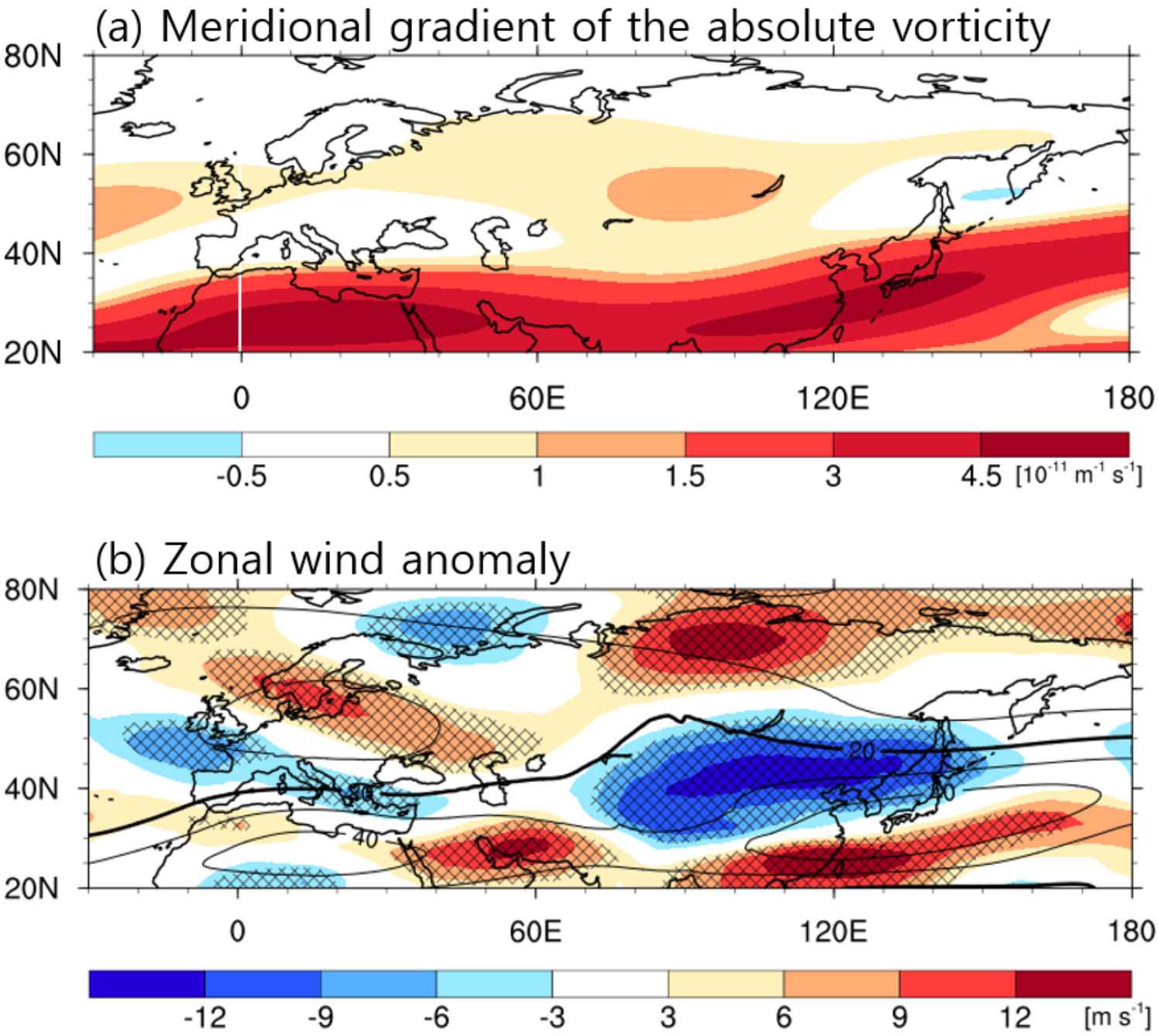

Figure 5

Possible causes for the cold condition. Upper-troposphere (200 hPa) (a) meridional gradient of the absolute vorticity (, 10^{-11} m^{-1} s^{-1}) climatology in April in the Mercator coordinate and (b) zonal wind (m s^{-1}) in April 2020 anomaly (shading) and climatology (contour, interval of 10 m s^{-1}). In (b), hatched areas represent the statistically significant regions at 90% confidence level.

Supplementary Files

This is a list of supplementary files associated with this preprint. Click to download.

- SupplementaryInformation02Dec2022.docx